Indian Journal of Chemical Technology
Vol. 30, September, 2023 pp. 693-704
DOI: 10.56042/ijct.v30i5.5200

Comparative study of ZnO-TiO_2 nanocomposites synthesized by ultrasound and conventional methods for the degradation of methylene blue dye

Dipak Giram[1], Arijit Das[1]* & Bharat Bhanvase[2]

[1]Department of Chemical Engineering, Visvesvaraya National Institute of Technology, Nagpur 440 010, Maharashtra, India
[2]Department of Chemical Engineering, Laxminarayan Institute of Technology, Nagpur 440 033, Maharashtra, India

*E-mail: arijitdas@che.vnit.ac.in

Received 5 March 2023; accepted 20 May 2023

ZnO-TiO_2 nanocomposites (ZTN) have been synthesized using both ultrasound-assisted and conventional methods. The characterization techniques like XRD, FTIR, BET, FESEM, EDS, and UV-visible confirmed that the ZTN is successfully formed. The photocatalytic activity and kinetics of the ZTN are assessed using methylene blue (MB) dye as a pollutant. Various factors such as synthesis processes, catalyst loading, initial dye concentration, temperature, and pH have been investigated to determine their impact on dye degradation. The ZTN synthesized with ultrasound exhibited superior photocatalytic activity compared to the conventionally synthesized ZTN. The highest dye degradation (97.69%) was observed under the optimum conditions of 1 g/L photocatalyst dosage, 20 ppm dye concentration, pH 10, and a temperature of 55°C. Additionally, the kinetic study revealed that the degradation of the dye by ZTN followed a second-order kinetic model.

Keywords: Kinetics, Methylene blue, Photocatalytic degradation, Ultrasound assisted synthesis, ZnO-TiO_2 nanocomposite

The growth of human populations and increasing industrialization have significantly reduced freshwater resources[1]. So, the demand for clean water has become an utmost priority worldwide[2,3]. Major industries like textiles, food, pharmaceuticals, cosmetics, and leather discharge the effluents into water bodies[4]. This effluent discharge causes severe contamination of water sources with various organic pollutants like phenols, antibiotics, organic dyes, and halogenated hydrocarbons[5]. These organic effluents are highly difficult to degrade and harm aquatic systems and human health[6]. So, getting rid of organic pollutants has become one of the most crucial issue for the environment. In recent years, several physical, chemical, and biological methods, such as adsorption, biodegradation, flotation, precipitation, oxidation, solvent extraction, evaporation, ion exchange, membrane filtration, and so on, have been used to detoxify organic contaminants[7]. Unfortunately, these conventional procedures are typically inadequate to eliminate the pollutants. As a result, an effective treatment method is required to address this issue.

Advanced oxidation processes (AOPs) are excellent treatment methods for organic pollutants. The mechanism of AOPs is to produce reactive species, such as the hydroxyl radical(OH•), that can rapidly and non-selectively oxidize organic molecules[8–10]. Among AOPs, photocatalytic technology has been widely used to degrade organic pollutants due to its advantages, which include high separation efficiency, cheap cost, safety, and the potential to utilize sunlight as their primary energy source[11]. In modern times, nanostructured semiconductors like TiO_2, ZnO, SnO_2, Fe_2O_3, ZrO_2, CeO_2, $BiVO_4$, CdS and ZnS have gained much interest in the photocatalytic process as photocatalysts[12].

Titanium dioxide (TiO_2) has become a promising and outstanding semiconductor metal oxide due to its best photostability, nontoxicity, low cost, and long-lasting photocatalytic behaviour[13]. TiO_2 has a band gap energy of 3 to 3.2 eV[14] and is observed in three crystalline forms, including rutile, anatase, and brookite. The anatase phase is advantageous and practicable due to its exceptional photocatalytic activity[15]. However, due to the large band gap and quick recombination of electron-hole interactions, the photocatalytic performance of TiO_2 is hampered. So, to overcome this drawback, multi-semiconductor hybrid nanocomposites could be used as a modification to enhance the photocatalytic performance of TiO_2[16]. Numerous researchers studied the nanocomposite of TiO_2 with other metal oxide semiconductors such as ZnO-TiO_2[16], WO_3-TiO_2[17], Fe_2O_3-TiO_2[18], SnO_2-TiO_2[19] and SiO_2-TiO_2[20].

ZnO is a strong semiconductor material with a band gap of 3.37 eV[21]. It has been intensively investigated for its photocatalytic action as it does not contain any harmful elements and is readily available[22,23]. As TiO_2 and ZnO have similar bandgap energies, identical photodegradation mechanisms, and excellent electron-hole pair separation, ZnO was chosen as an appropriate material to be coupled with TiO_2 in this work[24]. The coupling of ZnO and TiO_2 semiconductors was extensively used for the degradation of aqueous organic contaminants, having better photocatalytic efficiency than TiO_2 and ZnO alone[25]. The combination of the ZnO-TiO_2 metal oxides altered the band gap of the nanocomposite. This alteration results in enhanced charge separation and a reduction in the recombination rate of generated charge carriers. The increased lifespan of charge carriers is attributed to the improved diffusivity of both electrons and holes towards the interface between the oxide material and the organic compound. As a result, improved photocatalytic performance is achieved[26].

Numerous studies have synthesized the ZnO-TiO_2 nanocomposite (ZTN) using conventional methods, namely sol-gel, co-precipitation, and hydrothermal[16, 27–29]. However, conventional methods are time-consuming and expensive to carry out. It has been demonstrated that ultrasound is beneficial for the dispersion of tiny particles and the reduction of particle size[30]. In addition, it prevents the agglomeration of nanoparticles during the process[31]. Irradiation of the solution with ultrasonic waves results in the formation of cavities in the solution. After reaching a specific size, these cavities eventually collapse, releasing enormous amounts of energy. Under such severe conditions, several different kinds of chemical and physical reactions can take place. Because of this, it is possible to successfully construct nanostructured materials with the appropriate particle size[32].

This work used ultrasound and conventional methods (co-precipitation method) to synthesize ZTN photocatalysts. The methylene blue (MB) dye (the primary effluent of the textile industry) was used as a model pollutant to assess the photocatalytic activity of the produced nanocomposite in the presence of sunlight. In addition, the impact of catalyst loading, dye concentration, pH, temperature, and synthesis technique on the degradation of dye was tested. Furthermore, the photocatalysis mechanism and kinetic study of the ZTN were also studied in depth.

Experimental Section

Materials

Chemicals of analytical grade were procured for the synthesis of the nanocomposite. All the chemicals were utilized in their original form. Zinc acetate dihydrate, hydrochloric acid, sodium hydroxide, and isopropanol were purchased from Merck(India) Ltd. Titanium(IV) isopropoxide and MB dye were purchased from Sigma Aldrich. Throughout the experiments, distilled water and cleaned glassware were used to make the solutions.

Ultrasound synthesis of ZTN

Initially, a solution (A) was prepared by mixing titanium(IV) isopropoxide (5 mL) with isopropanol (50 mL). The solution (B) was made by dissolving 2 g of zinc acetate dihydrate in 10 mL distilled water. Solution A and B were poured into a beaker, and the mixture was sonicated by ultrasound (Dakshin, 180 W, 22 kHz, 4 sec on, 5 sec off) for 15 min. The resulting solution was infused with 50 mL of NaOH solution (concentration 1.3555 mol/L) at a rate of 5 mL/min, followed by 20 min of sonication. After completion of sonication, the solution (reaction mass) was filtered, cleaned, and dried in a hot air oven (Bio Technics India) at 100°C for 5 h to get ZTN powder. All the experiments were performed in duplicate.

Conventional synthesis of ZTN

To synthesize the ZTN powder by a conventional method, titanium (IV) isopropoxide (5 mL) was first dissolved in isopropanol (50 mL). After that, 2 g zinc acetate dihydrate was added to 10 mL distilled water to prepare the zinc acetate solution. A conventional stirring method was employed to mix zinc acetate solutionsand titanium isopropoxide solutions for 3 h in a beaker. Finally, 50 mL NaOH solution (concentration 1.35 mol/L) was added dropwise to the stirred solution, followed by 5 h of stirring. The reaction mass was collected, filtered, and dried at 100°C for 5 h, then crushed in a mortar pestle to obtain ZTN powder.

Photocatalytic degradation of MB dye

The photocatalytic activity of ZTN was monitored with the degradation of the aqueous MB dye solution. Experiments on dye degradation were started around 11 a.m. in the month of May, when variations in solar intensity were minimal. In a typical experiment, a 100 mL aqueous MB dye solution with a concentration of 40 ppm was taken into a conical

flask. A fixed amount of ZTN photocatalyst was added to the MB solution. The resulting suspension was vigorously stirred for 30 min in darkness to attain adsorption-desorption equilibrium between dye and ZTN photocatalyst and then transferred to a photocatalytic reactor. This photocatalytic reactor was kept outside under the sunlight, and constant mixing of the contents in the reactor was ensured using a magnetic stirrer. The samples were collected at regular intervals, centrifuged immediately after collection, and then examined using a UV-visible spectrophotometer to determine the respective concentration of dye. The wavelength of 665 nm was chosen as it shows the highest absorbance of an aqueous MB solution. Eq. (1) was used to estimate the percentage degradation of MB.

$$\%\ Degradation = \frac{C_0 - C}{C_0} \times 100 \quad \ldots (1)$$

where C_0 represents the initial dye concentration at time t =0 and C represents the dye concentration at time t = t. The degradation rate of ZTN photocatalyst was studied with a variety of experimental parameters, including the synthesis method (ultrasound-assisted and conventional synthesis), catalyst dosage (0.2 to 2 g/L), initial MB dye concentration (20 to 100 ppm), pH (3, 5, 7, 8 and 10), and temperature (35 to 55 °C).

Characterization of prepared ZTN

The XRD (Rigaku Mini-Flex 600 equipment) was used to investigate the crystallite structure, crystallite size, and phase composition of the ZTN. An FTIR (Shimadzu-IR Affinity-1, Japan) was used to examine the chemical bonds and molecular composition of ZTN. FESEM and EDS were used to investigate the shape, morphology, and composition of elements of ZTN (Carl Zeiss, Germany). A UV-visible spectrophotometer (LABINDIA, Model: UV-3200) was employed for the measurement of the concentration of an aqueous MB dye solution.

Results and Discussion

Characterization of ZTN synthesized by ultrasound and conventional methods

XRD analysis

Fig. 1 depicts the XRD pattern of ZTN synthesized by ultrasound and conventional methods. The peaks at 2θ = 31.83°, 34.54°, 36.3°, 56.71°, 63.02°, 68.1°, and 69.02° correspond to the ZnO crystal planes (1 0 0), (0 0 2), (1 0 1), (1 1 0), (1 0 3), (1 1 2), and (2 0 1),

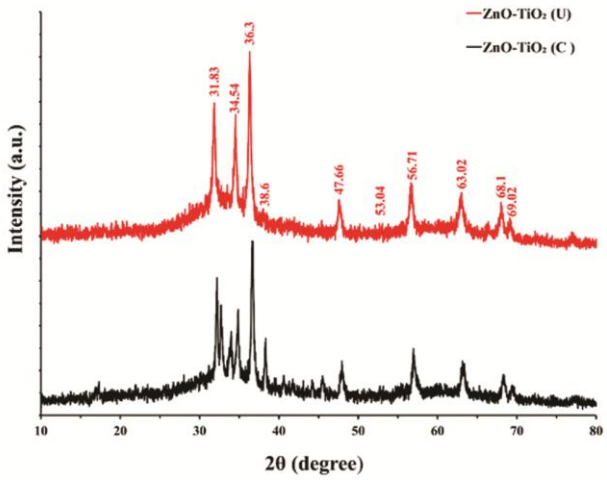

Fig. 1 — XRD patterns of ZTN synthesized by ultrasound and conventional methods

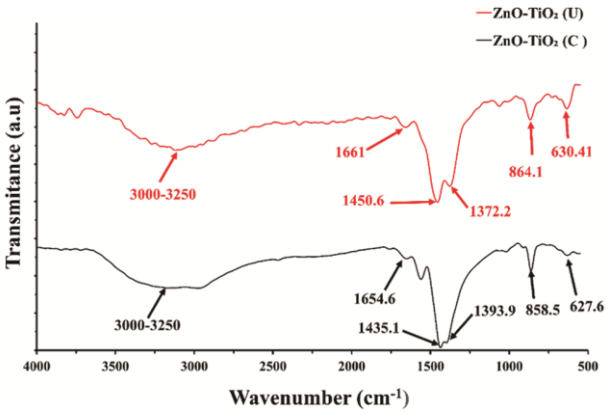

Fig. 2 — FTIR spectra of ultrasonically and conventionally synthesized ZTN

respectively[33,34]. The characteristic peaks at 38.66°, 47.66°, and 53.04° could be attributed to the anatase phase[35,36]. Thus, the XRD characterization of the produced nanocomposite showed the existence of only the anatase phase of TiO_2.The crystallite sizes of ZTN synthesized by both methods were determined using the Debye- Scherrer formula:

$$D = \frac{\lambda K}{\beta \cos \theta} \quad \ldots (2)$$

where D represents crystallite size, K=0.9 (Scherer's constant), λ = 1.5406 Å (wavelength of X-ray), β is Full width at half maximum (FWHM) and θ is the angle of diffraction. The nano-crystallite sizes of ZTN (ultrasound) and ZTN (conventional) were calculated as22.48 nm and 25.39 nm, respectively.

FTIR analysis

Fig. 2 depicts the FTIR spectra of ultrasonically and conventionally synthesized ZTN within 4000 to

500 cm^{-1}. It was observed that the FTIR spectra of ZTN synthesized by both methods were almost identical. The band near 864.1 cm^{-1} corresponds to Ti-O-Ti and TiO vibrations[37], while the bands between 500 and 750 cm^{-1}indicate the existence of ZnO bonds[38]. In addition, the C=O and O-H bending vibrations are assigned to the bands at 1393.9 and 1654.6cm^{-1}, respectively. Furthermore, bands above 3000 cm^{-1} show the existence of a hydroxyl group in the synthesized ZTN.

UV-visible analysis

The light absorbance characteristics of the ZTNs were examined by UV-visible spectroscopy, and the resulting spectra are shown in Fig. 3(a). The structure of TiO_2 and ZnO was confirmed by the UV absorption peak at 254 and 364 nm, respectively. The ZTN shows two absorption peaks: one is in the UV range, and the second peak is in the visible range. The maximum absorption of the UV region was derived from TiO_2, while the absorption of the visible range was generated from ZnO. The band gap energy of ZTN was estimated using the Tauc plot method.

$$(\alpha h\nu)^{\gamma} = A(h\nu - E_g) \quad \ldots (3)$$

Where α is the absorption coefficient, h is the plank constant, ν is photon's frequency, A is the proportionality constant, γ denotes the nature of the electronic transition, and E_g represents the energy gap. γ=1/2 and γ=2 for indirect and direct transitions. Thus, extrapolating the linear region on the abscissa yields the bandgap energy of the nanocomposite. The estimated band gap values of ZTN for the ultrasound and conventional methods were 3.16eV and 3.31eV, respectively (Fig. 3(b)). This reduction in band gap improved the optical characteristics of the ZTN synthesized by the ultrasound method, which can be favourable for photocatalytic applications.

FESEM and EDS analysis

The morphological characteristics of ZTN were examined using FESEM (Fig. 4) It has been observed that the morphology of TiO_2 and ZnO is distinct in both cases. Fig. 4(a) shows irregular spherical TiO_2 nanoparticles and elongated ZnO nanoparticles. The cavitation phenomenon causes the scattering of nanoparticles with significantly smaller reduced sizes. However, in Fig. 4(b), the ZTN is agglomerated unsymmetrically. This aggregation decreases the surface area. The elemental compositions of ZTN produced using ultrasound and conventional techniques are shown in Fig. 4(c and d), respectively. The EDS study revealed the presence of Zn, Ti, and O elements. The Zn element comes predominantly from ZnO, Ti element comes from TiO_2 and O comes from ZnO and TiO_2. The presence of zinc, titanium, and oxygen all pointed to the synthesis of ZTN.

BET analysis

Brunauer–Emmett–Teller (BET) was used the surface properties like surface area and pore volume distribution of ZTN synthesized by both methods. The investigation was executed over nitrogen gas at 77.35 K. The BET surface area for ZTN was 6.405 m^2/g (ultrasound) and 1.642 m^2/g (conventional), respectively. Further, the pore volume of ZTN was estimated as 0.0011 cc/g (ultrasound) and 0.0001 cc/g (conventional), respectively. The surface area of ultrasonically prepared ZTN was higher than that of conventionally synthesized ZTN. This is because using ultrasound for synthesis leads to the formation of the cavitation phenomenon. That cavitation phenomenon results in the delamination of particle size into smaller particles, increasing surface area. This high surface area increases the exposure of the nanocomposite to photocatalysis reactions,resulting in more particle collisions.

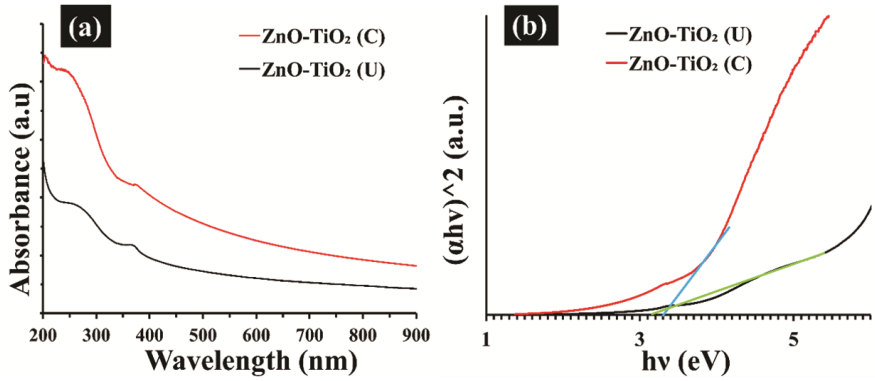

Fig. 3 — (a) UV-visible absorption spectra (b) band gap energy calculation of ZTN synthesized by ultrasound and conventional methods

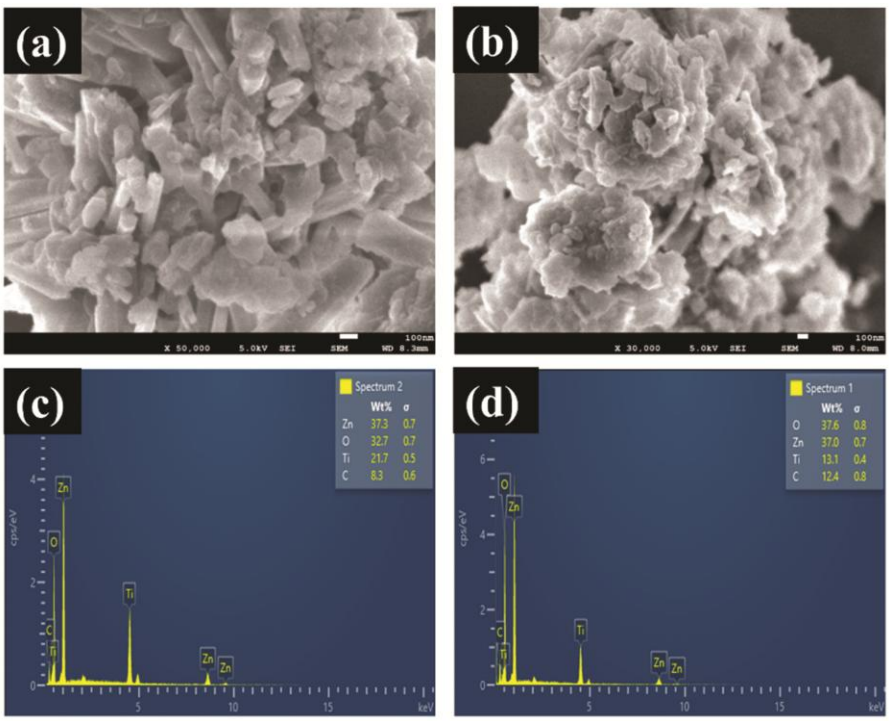

Fig. 4 — FESEM and EDS analysis of ZTN synthesized by ultrasound (a and c) and conventional (b and d) methods

Role of ultrasound on the synthesis of ZTN

In the synthesis of ZTN by a conventional method, the reaction time required was 8 h 10 min, whereas the reaction time required for the synthesis of ZTN using an ultrasound method was just 45 min. This confirmed that the completion of the reaction ultrasound method requires less time than the conventional method. When ultrasound waves (20 kHz) were incorporated into reaction media, the molecules oscillated, which resulted in a change in the average distance of molecules. This was due to the bubble formation, growth formation, and collapse of bubbles in reaction media. The bubbles collapsing leads to the generation of substantial local temperatures (>5000K) and local pressure (>20MPa)*(hot spots)*[39]. The thermal effect of these hot spots is the main principle behind the use of ultrasound. In addition to the thermal effect, the collapse of bubbles also creates strong shearing forces. Several physical and chemical changes occur due to the collapse of these bubbles. In this work, pulse ultrasonication was used for the synthesis of ZTN. This pulsed ultrasonication can alter an ultrasound bubbles oscillation and growth dynamics[40]. Further, pulsed ultrasonication also reduces wave scattering induced by bubbles clouds, resulting in energy conservation. In the continuous mode of ultrasonication, a portion of acoustic energy was lost and dissipated into vibrations and heat[40,41]. The result obtained from the BET confirms that ultrasonically prepared ZTN has a higher surface area (6.405 m^2/g) than conventionally synthesized (1.642 m^2/g) ZTN. This is due to high-velocity interparticle collisions that break the particles into smaller sizes. Also, FESEM confirms that the ultrasound method avoids the aggregation of nanoparticles.

Photocatalytic activity ZTN

The pseudo-first-order (PFO) kinetic model, often utilized for dye degradation kinetics, is inappropriate for determining the effect of experiment parameters. As a result, the second-order kinetic model has been tested for degradation. The PFO and second-order kinetic models are represented in Eqs. (4) and (5), respectively.

$$ln\ \frac{C_0}{C} = k_1 t \quad \ldots (4)$$

$$\frac{1}{C} = k_2 t + \frac{1}{C_0} \quad \ldots (5)$$

where C_0 represents the concentration of dye present initially at time t=0 while C represents the concentration of dye at time t=t and k_1(min^{-1}) and k_2($Lmole^{-1}$ sec^{-1}) are rate constants for the pseudo-first-order and second-order kinetics, respectively.

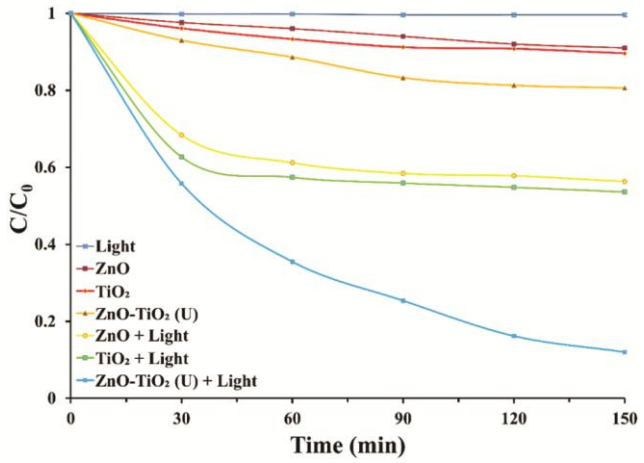

Fig. 5 — Comparison of MB dye degradation by different processes (catalyst loading= 0.5 g/L, initial dye concentration = 40 ppm, pH= 7, temperature= 35°C)

Graphs of ln (C_0/C) vs. time (t) and $1/C$ vs. time (t) values were plotted using different experimental parameters such as catalyst loading, initial dye concentration, initial pH, and temperature. The k_1 and k_2 values were determined from the slopes of the graphs. The graph's linearity and R^2 values suggest that the second-order kinetics are consistent with the photocatalytic degradation of MB dye on the ZTN photocatalyst.

Comparison of MB dye degradation by different processes

Fig. 5 shows the degradation of MB dye (initial concentration of 40 ppm) using different processes. Initially, the degradation of MB without a catalyst was studied for comparison. The results revealed that no degradation was achieved after 150 min of photolysis, indicating that photolysis alone is an ineffective approach for the degradation of dye under sunlight. Also, the degradation of dye with different catalysts (absence of light) was studied. As illustrated in Fig. 5, the adsorption of dye molecules onto TiO_2, ZnO, and ZTN resulted in 9%, 10.4% and 19.3% removal of dye, respectively. In the photocatalysis process, TiO_2 (43.7%), ZnO (46.4%) and ZTN (88.02%) showed better results as compared to adsorption due to the production of hydroxyl radicals (oxidizing agent). The results showed that the photocatalysis of dye with ZTN was superior to that of pure TiO_2 and ZnO due to the reduction in band gap. However, the photocatalytic degradation of pure TiO_2 and ZnO under sunlight illumination is low due to the larger band gap (3.2 eV), which results in lower absorption of visible light. So, the best outcomes were seen with ZTN, making it the preferred choice for further experiments.

Effect of catalyst loading

One of the key criteria affecting the performance of the photocatalytic process is the amount of catalyst loading. Fig. 6 illustrates several different catalyst dosages based on an initial dye concentration of 40 ppm. Temperature and pH were maintained at 35°C and 7, respectively, while the dosage of the selected catalyst ranged from 0.2 to 2 g/L. Excessive usage of the catalyst results in the formation of aggregate, which lowers the performance of the photocatalyst[42].

Fig. 6(a) depicts the effect of loading of ZTN synthesized by the ultrasound method. The catalyst dose was 0.1, 0.5, 1, and 2 g/L. As photocatalyst dosage was raised from 0.2 g/L to 1 g/L, the percentage of MB dye degradation raised from 55.52 to 93.25% at 150 min. This is due to the increment in the number of active sites in the photocatalyst, which are responsible for enhancing dye degradation[43]. As the catalyst dose was raised from 1 to 2 g/L, the degradation marginally increased from 93.25 to 93.83%. This is because when the photocatalyst loading increases, the reaction mixture becomes opaque. Increasing the dose from 1 to 2 g/L didn't significantly impact dye degradation, so the 1 g/L dose was considered optimum. The PFO kinetics and second-order kinetics of the MB dye degradation while exposed to sunlight are depicted in Fig. 6(b and c). The effect of catalyst loading of ZTN synthesized by the conventional method is shown in Fig. 6(d). The amounts of catalyst 0.1, 0.5, 1, and 2 g/L were used, corresponding to the overall degradation of 52.94, 72.75, 85.31, and 86.96%, respectively.

The highest photocatalytic degradation of MB dye achieved with ZTN photocatalysts prepared with ultrasound and conventional techniques was 93.83% and 85.96%, respectively. This is attributed to the use of the ultrasound technique for the synthesis of ZTN which has a smaller particle size and a higher surface area, which allows carriers to quickly access the surface and engage in photoactivity. The chance of charge recombination outside the barrier zone increases with crystallite size, resulting in decreased photocatalytic activity. As a result, the ultrasound-assisted method was preferred over the conventional method in terms of high photocatalytic activity.

Effect of initial dye concentration

Fig. 7(a) represents the influence of initial dye concentrations (20 to 100 ppm) on its degradation at

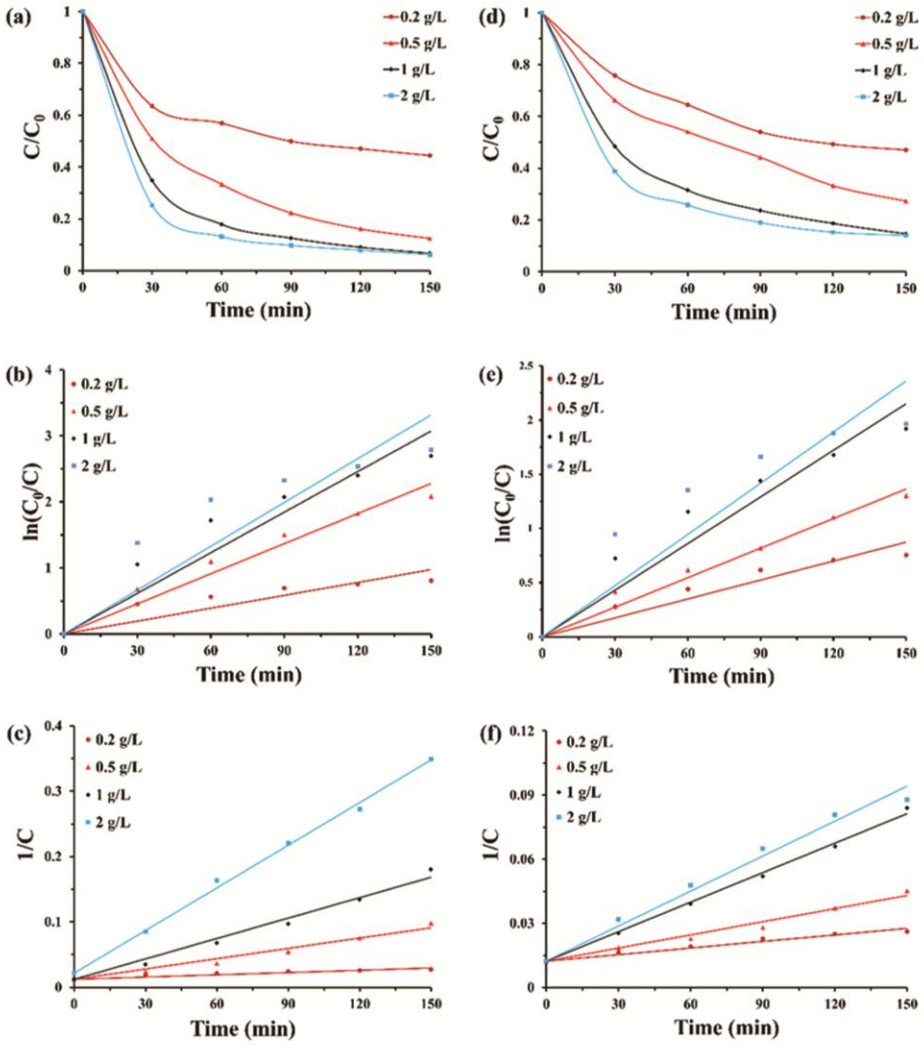

Fig. 6 — Effect of catalyst loading on dye degradation (a and d), pseudo first order (b and e) and Second order kinetic models (c and f) using ZTN photocatalyst synthesized by ultrasound and conventional methods, respectively. (initial dye concentration = 40 ppm, volume of batch = 100 mL, pH = 7 and temperature = 35℃)

35°C with a fixed optimal photocatalyst dosage of 1 g/L and a constant pH of 7. It has been observed that the percentage degradation of dye decreases with an increase in dye concentration. At the total irradiation time of 120 min, the degradation of the 20 ppm dye concentration was determined to be 97.48% and dropped to 75.82% for 100 ppm. This is attributed to the increase in the dye concentration, and the adsorption of more dye molecules on the photocatalyst surface, resulting in fewer photons reaching the catalyst surface. Consequently, fewer $OH^{\bullet}$ radicals were produced, and a lower percentage of degradation was obtained[38]. Figs. 7(b) and (c) shows PFO and the second-order kinetics of the degradation of MB dye, respectively.

Effect of initial pH

pH is considered the most crucial factor for dye degradation because the catalyst's surface charge relies on the pH of the solution. The solution's pH can influence dye molecules' adsorption on the catalyst surface[44]. Fig. 8(a) depicts the impact of pH (3, 5, 7, 8 and 10) on dye degradation while other factors such as catalyst loading of 1 g/L, initial dye concentration of 20 ppm, and temperature of 35℃ were held constant. It was found that the degradation was higher in basic conditions than in acidic conditions. At acidic pH (3 and 5), the MB dye degradation percentage was determined as 10.18% and 59.91%, respectively, after 120 min of sunlight. It was found that the degradation of dye increased linearly with pH. At the end of

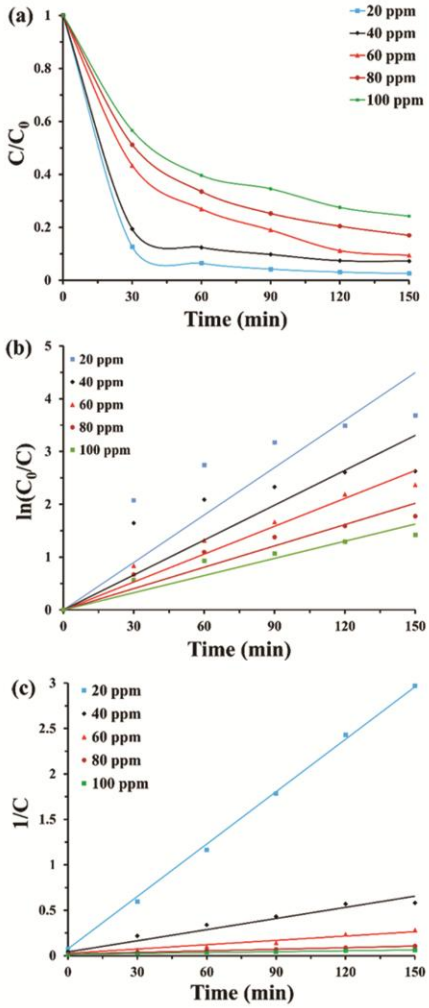

Fig. 7 — (a) Effect of initial dye concentration on dye degradation using ZTN synthesized by ultrasound method (catalyst loading = 1 g/L, volume of batch = 100 mL, pH = 7 and temperature = 35°C), (b) PFO kinetic model and (c) Second-order kinetic model

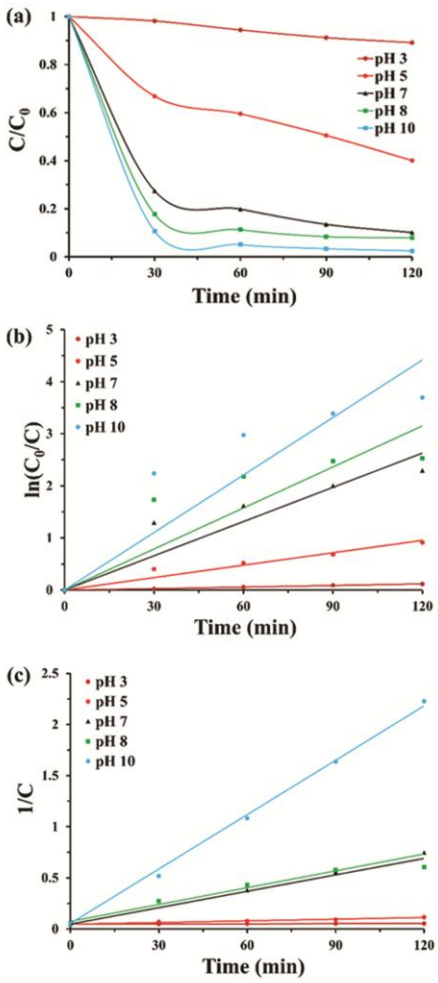

Fig. 8 — (a) Effect of pH on MB dye degradation using ZTN synthesized by ultrasound method (catalyst loading = 1 g/L, volume of batch = 100 mL, initial dye concentration = 20 ppm and temperature = 35°C), (b) PFO kinetic model and (c) Second-order kinetic model

120 min, results showed that degradation reached values of 89.99%, 92.02% and 97.51% for pH 7, 8 and 10, respectively. The dye degradation was likewise higher (97.51%) at the end of 120 minutes at basic pH 10. At acidic pH (3 and 5), dye degradation was lower due to positive holes forming at lower pH levels and acting as the main oxidation species[44]. However, at high pH (7, 8, and 10), the degradation of dye was more significant because hydroxyl radicals ($OH^{\bullet}$) created at neutral or higher pH behave as predominant oxidation species[45]. In an alkaline solution, $OH^{\bullet}$ radicals are easier to produce by oxidizing hydroxide ions present on the surface of TiO_2, resulting in an enhancement in degradation efficiency. Fig. 8(b) and (c) show PFO kinetics and second-order kinetics.

Effect of Temperature

Fig. 9(a) shows the effect of temperature on MB dye degradation. The solution temperature was maintained with a magnetic heater between 35-55°C while the other parameters were kept constant. The degradation of MB dye continuously increases as the temperature rises. This enhancement is attributed to two reasons: (1) increased temperature results in an enhancement in collision frequency between dye molecules and catalyst sites, resulting in higher degradation rates of the dyes; (2) as the temperature rises, bubbles begin to develop within the solution, which ultimately leads to the production of free radicals[44,46]. The result shows that the highest 97.69% degradation was obtained at 55°C. Fig. 9(b) and (c) show PFO and second-order kinetics.

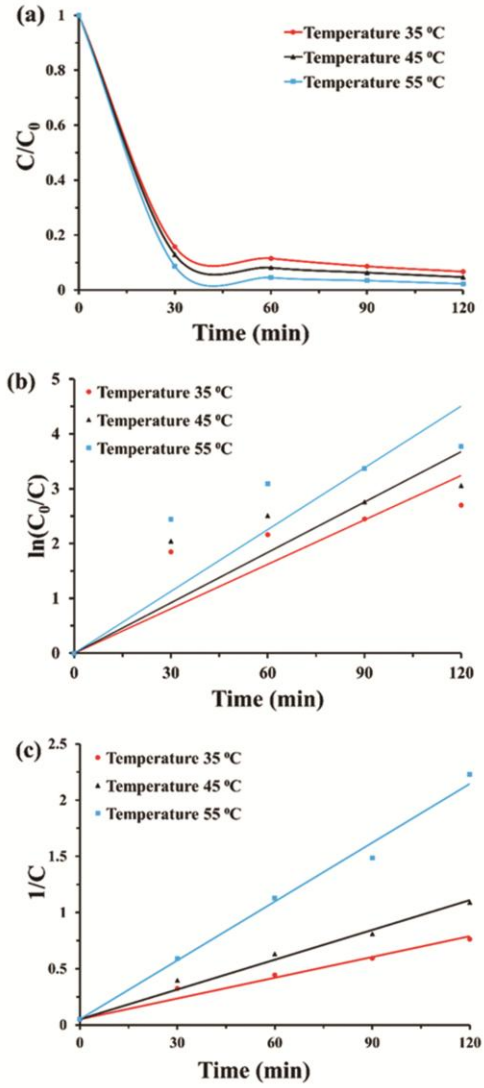

Fig. 9 — (a) Effect of temperature on dye degradation using ZTN synthesized by ultrasound method (catalyst loading =1 g/L, initial dye concentration = 20 ppm, volume of batch = 100 mL, and pH = 7), (b) PFO kinetic model and (c) Second-order kinetic model

Arrhenius equation was employed to investigate the effect of temperature on the second order kinetic model for MB dye degradation in the following equation:

$$k = k_0 \exp\left(\frac{-E}{RT}\right) \quad \ldots (6)$$

Eq. (6) represents that k values are inversely proportional to temperature and can be converted in linear form by taking natural logarithms on both sides.

$$lnk = lnk_0 - \left(\frac{E}{RT}\right) \quad \ldots (7)$$

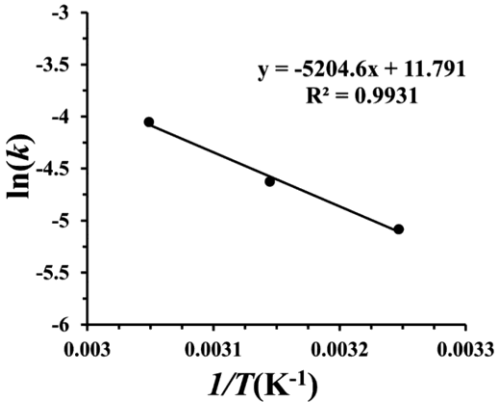

Fig. 10 — Plot of ln(k) Vs. 1/T

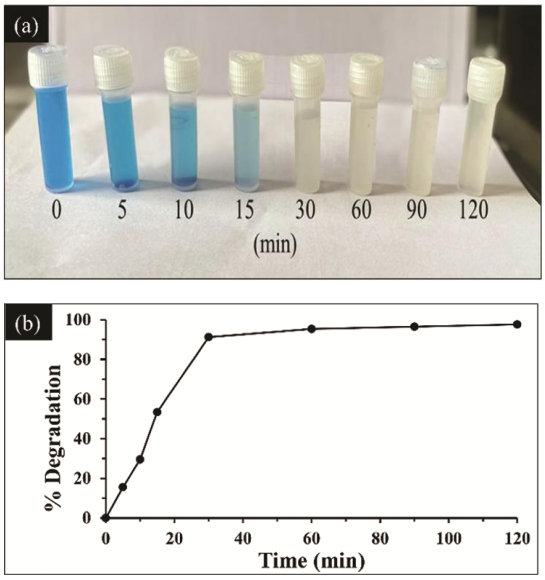

Fig. 11 — (a) Photographic images of dye degradation at optimized condition and (b) Effect of optimized condition on dye degradation using ZTN synthesized by ultrasound method (catalyst loading = 1 g/L, volume of batch = 100 mL, initial dye concentration = 20 ppm, pH = 10 and temperature = 55°C)

The activation energy (E) value was estimated from the graph by plotting ln(k) on the Y-axis and 1/T on the X-axis (Fig. 10). The estimated activation energy (E) value for the degradation of MB dye over ZTN photocatalyst was 43.25 kJ/mol. Fig. 11(a) shows the photographs of dye degradation at optimized condition Fig. 11(b) shows the maximum percentage degradation of MB dye on ZTN photocatalyst while other optimized parameters such as catalyst loading of 1g/L, 20 ppm initial dye concentration, pH 10, and 55°C temperature were kept constant. The result showed that 91.32% of MB dye degradation occurred within 30 min and reached a maximum degradation percentage of 97.69% at the end of 120 min.

Adsorption and degradation study at optimized conditions

To investigate the kinetics of adsorption and degradation of MB dye, experiments were conducted under optimized conditions. The optimized conditions included a catalyst loading of 1 g/L, an initial dye concentration of 20 ppm, a pH of 10, and a temperature of 55°C. Initially, preliminary experiments were performed in the absence of light to establish the equilibrium state between dye and ZTN. The experimental findings, as illustrated in Fig. S1(a) (Supplementary Information), demonstrate that the adsorption-desorption equilibrium of MB dye was achieved in a time period of 30 min. During this period, the adsorption capacity of ZTN for MB dye was measured to be approximately 14.6%.

Fig. S1(b) demonstrates the impact of adsorption and degradation on the removal of MB dye under optimized conditions. As illustrated in Fig. S1(b), after a total irradiation time of 150 min, the removal of the dye concentration reached 97.02%. However, during the initial 30 min (in the dark), the adsorption of MB onto ZTN was relatively lower compared to the total removal of MB dye, suggesting that degradation played a more dominant role than adsorption. Therefore, the primary factors contributing to the removal of MB dye were the comparatively slower adsorption and the relatively faster degradation.

Additionally, the time-dependent degradation of MB using ZTN photocatalyst under optimized conditions is demonstrated in Fig. S2 given in the (UV-visible absorption spectra) Supplementary Information. The degradation process was monitored by analyzing the changes in the absorbance spectrum of the MB before and after treatment. The results exhibit that MB has a characteristic absorption peak at a 665 nm (λ_{max}) wavelength in their UV-Vis spectrum before degradation (time = 0 min). However, after 150 min, the characteristic absorption peak at 665 nm disappeared, signifying the successful degradation of MB.

Degradation mechanism of ZTN photocatalyst

Fig. 12 illustrates the dye (MB) degradation mechanism of ZTN (ZnO-TiO_2 nanocomposite) under sunlight exposure. As ZTN is irradiated with sunlight, which has photon energy equal to or greater than the band gap energy of the material, the ZnO and TiO_2 photocatalysts are stimulated and generate electrons and holes. Specifically, an electron in the valence band (VB) of both ZnO and TiO_2 is excited and moves to the conduction band (CB), leaving behind a hole in the VB. The CB electrons of ZnO are migrated to the CB of TiO_2. Likewise, the holes are migrating from the VB of TiO_2 to the VB of ZnO. This migration process reduces the recombination of charge, thereby decreasing the rate of recombination. This reduction in the recombination rate improves the photocatalytic performance of ZTN. The oxygen molecules adsorbed on the photocatalyst interact with electrons of ZnO and TiO_2 to form oxygen

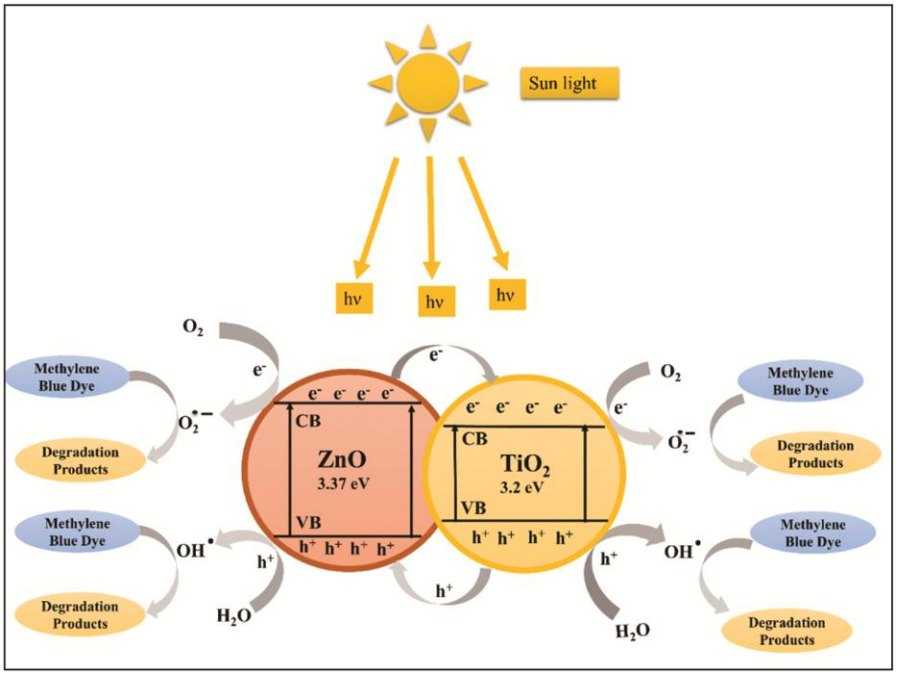

Fig. 12 — Dye degradation mechanism of ZTN photocatalyst

radicals ($O_2^{-\bullet}$). Moreover, Surface hydroxyl groups react with holes in the valence band of ZnO and TiO_2, leading to the formation of highly reactive hydroxyl ($OH^{\bullet}$) radicals. Both hydroxyl radicals ($OH^{\bullet}$) and superoxide radicals($O_2^{-\bullet}$), are responsible for the dye degradation[28,29,47].

The degradation mechanism of the dye molecule on ZTN can be summarized by the following equations (8) to (12).

$$ZnO - TiO_2 + h\nu \leftrightarrow ZnO - TiO_2[(h^+ + (e^-)] \quad \ldots (8)$$

$$ZnO - TiO_2(e^-) + O_2 \rightarrow (O_2^{-\bullet}) + H^+ \quad \ldots (9)$$

$$ZnO - TiO_2(h^+) + H_2O \rightarrow (OH^{\bullet}) + H^+ \quad \ldots (10)$$

$$(OH^{\bullet}) + MB\ dye \rightarrow Degradation\ products \quad \ldots (11)$$

$$O_2^{-\bullet}) + MB\ dye \rightarrow Degradation\ products \ldots (12)$$

Conclusion

ZTN was successfully synthesized by ultrasound and conventional methods. The successful synthesis of ZTN was confirmed by XRD, FTIR, UV-visible, FESEM, EDS, and BET techinques. MB dye was chosen as the model pollutant to assess the photocatalytic activity of prepared ZTN. The results revealed that ultrasonically prepared ZTN exhibits outstanding photocatalytic behavior over MB dye degradation under sunlight. The degradation was found to increase with raising the catalyst loading to 1 g/L and then reduce at a higher catalyst dosage. At the fixed quantity of catalyst dosage, MB degradation was reduced as an increment in initial dye concentration. The result also indicated that the degradation of MB dye was superior in the basic medium than acidic medium. The maximum degradation of MB treatment was observed to be 97.69% under the optimum conditions of 120 min of irradiation, 1g/L photocatalyst dosage, 20 ppm initial dye concentration, pH 10, and temperature of 55℃. The further kinetic study proved that dye degradation on ZTN follows the second-order kinetic model.

Acknowledgements

The authors acknowledge the contribution of Visvesvaraya National Institute of Technology, Nagpur, India, for providing financial support, experimental facilities, and other necessary facilities to carry out this research work.

Supplementary Information

Supplementary information is available in the website http://nopr.niscpr.res.in/handle/123456789.

References

1 Jain K, Patel A S, Pardhi V P & Flora S J, *Molecules*, 26 (2021) 1797.
2 Khalid N R, Majid A, Tahir M B, Niaz N A & Khalid S, *Ceram Int*, 43 (2017) 14552.
3 Gholamian S, Hamzehloo M & Farrokhnia A, *J Environ Chem Eng*, 9 (2021) 104937.
4 Isai K A & Shrivastava V S, *S N Appl Sci*, 1 (2019) 1.
5 Ma R, Zhang S, Wen T, Gu P, Li L, Zhao G, Niu F, Huang Q, Tang Z & Wang X, *Catal Today*, 335 (2019) 20.
6 Ahmed S, Khan F S A, Mubarak N M, Khalid M, Tan Y H, Mazari S A, Karri R R & Abdullah E C, *J Environ Chem Eng*, 9 (2021) 106643.
7 Crini G & Lichtfouse E, *Environ Chem Lett*, 17 (2019) 145.
8 Yegane B M, Vosoughi M, Sadeghi H, Mokhtari S A & Mehralipour J, *Int J Environ Anal Chem*, 102 (2022) 757.
9 Ghazanfari S Z, Jaafari J, Ashrafi S D & Taghavi K, *Int J Environ Anal Chem*, 00 (2021) 1.
10 Hayoune A, Akkari H, Vaiano V, Morante N, Sannino D & Madjene F, *Int J Environ Anal Chem*, 00 (2021) 1.
11 Rajaraman T S, Parikh S P & Gandhi V G, *Chem Eng J*, 389 (2020) 123918.
12 Dlamini M C, Maubane-Nkadimeng M S & Moma J A, *J Environ Chem Eng*, 9 (2021) 106546.
13 Rashidzadeh B, Fathalipour S, Hosseini S P & Bazazi S, *Int J Environ Anal Chem*, 00 (2022) 1.
14 Chkirida S, Zari N, Achour R, Qaiss A el kacem & Bouhfid R, *Environ Sci Pollut Res*, 28 (2021) 14018.
15 Asadzadeh P H, Fattahi M & Khosravi-Nikou M, *Sci Rep*, 11 (2021) 1.
16 Upadhyay G K, Rajput J K, Pathak T K, Kumar V & Purohit L P, *Vacuum*, 160 (2019) 154.
17 El-Yazeed W S A & Ahmed A I, *Inorg Chem Commun*, 105 (2019) 102.
18 Fawzi S K O & Palaniandy P, *Environ Technol Innov*, 21 (2021) 101230.
19 Sharma S, Kumar N, Makgwane P R, Chauhan N S, Kumari K, Rani M & Maken S, *Inorganica Chim Acta*, 529 (2022) 120640.
20 Rasheed T, Adeel M, Nabeel F, Bilal M & Iqbal H M N, *Sci Total Environ*, 688 (2019) 299.
21 Weldegebrieal G K, Dube H H & Sibhatu A K, *Int J Environ Anal Chem*, 00 (2021) 1.
22 Chaudhary K, Shaheen N, Zulfiqar S, Sarwar M I, Suleman M, Agboola P O, Shakir I & Warsi M F, *Synth Met*, 269 (2020) 116526.
23 El-Shazly A N, Rashad M M, Abdel-Aal E A, Ibrahim I A, El-Shahat M F & Shalan A E, *J Environ Chem Eng*, 4 (2016) 3177.
24 Menon N G, Tatiparti S S V & Mukherji S, *Colloids Surfaces A Physicochem Eng Asp*, 565 (2019) 47.
25 Wang X, Wu Z, Wang Y, Wang W, Wang X, Bu Y & Zhao J, *J Hazard Mater*, 262 (2013) 16.
26 Mohamadi Z N, Koozegar K B & Mazinani B, *Mater Technol*, 35 (2020) 281.

27 Li X, Wang C, Xia N, Jiang M, Liu R, Huang J, Li Q, Luo Z, Liu L, Xu W & Fang D, *J Mol Struct*, 1148 (2017) 347.

28 Ali M M, Haque J, Kabir M H, Kaiyum M A & Rahman M S, *Results Mater*, 11 (2021) 100199.

29 Akhter P, Nawaz S, Shafiq I, Nazir A, Shafique S, Jamil F, Park Y & Hussain M, *Mol Catal*, 535 (2023) 112896.

30 Choudhari A, Bhanvase B A, Saharan V K, Salame P H & Hunge Y, *Ceram Int*, 46 (2020) 11290.

31 Kale D P, Deshmukh S P, Shirsath S R & Bhanvase B A, *Optik (Stuttg)*, 208 (2020) 164532.

32 Bhanvase B A, Sonawane S H, Pinjari D V, Gogate P R & Pandit A B, *Chem Eng Process Process Intensif*, 85 (2014) 168.

33 Talam S, Karumuri S R & Gunnam N, *ISRN Nanotechnol*, 2012 (2012) 1.

34 Khorsand Z A, Razali R, Abd M W H & Darroudi M, *Int J Nanomed*, 6 (2011) 1399.

35 Ijadpanah-Saravy H, Safari M, Khodadadi-Darban A & Rezaei A, *Anal Lett*, 47 (2014) 1772.

36 Bagheri S, Shameli K & Abd Hamid S B, *J Chem*, 2013 (2013) 848205.

37 Potle V D, Shirsath S R, Bhanvase B A & Saharan V K, *Optik (Stuttg)*, 208 (2020) 164555.

38 Satdeve N S, Ugwekar R P & Bhanvase B A, *J Mol Liq*, 291 (2019) 111313.

39 Deshmukh S P, Kale D P, Kar S, Shirsath S R, Bhanvase B A, Saharan V K & Sonawane S H, *Nano-Struct Nano-Objects*, 21 (2020) 100407.

40 Teh C Y, Wu T Y & Juan J C, *Chem Eng J*, 317 (2017) 586.

41 Bhanvase B A, Veer A, Shirsath S R & Sonawane S H, *Ultrason Sonochem*, 52 (2019) 120.

42 Balcha A, Yadav O P & Dey T, *Environ Sci Pollut Res*, 23 (2016) 25485.

43 Shende T P, Bhanvase B A, Rathod A P, Pinjari D V & Sonawane S H, *Ultrason Sonochem*, 41 (2018) 582.

44 Rafiq A, Ikram M, Ali S, Niaz F, Khan M, Khan Q & Maqbool M, *J Ind Eng Chem*, 97 (2021) 111.

45 Akpan U G & Hameed B H, *J Hazard Mater*, 170 (2009) 520.

46 Fulzele N N, Bhanvase B A & Pandharipande S L, *Mater Chem Phys*, 292 (2022) 126809.

47 Kumar P, Kundu V S, Kumar S, Saharan B, Kumar V & Chauhan N, *Bionanoscience*, 7 (2017) 574.